Removal of azodyes using natural phosphate doped by titanium dioxide (NP-TiO$_2$) nanoparticles

M. Joudi[a], H. Hafdi[a], J. Mouldar[a], H. Nasrellah[a], B. Hatimi[a], M.A. El Mhammedi[b], M. Bakasse[a,*]

[a]_Laboratoire de Chimie Organique Bioorganique et Environnement, Faculté de Sciences, Université Chouaib Doukkali, Morocco,_
Tel. +212662835969; email: minabakasse@yahoo.fr (M. Bakasse), Tel. +212659247610; email: joudi.doct@gmail.com (M. Joudi),
Tel. +212645289301; email: hafdihouyem@gmail.com (H. Hafdi), Tel. +212627576202; email: mouldar.jihane@gmail.com (J. Mouldar),
Tel. +212666713132; email: nasrellah205@yahoo.fr (H. Nasrellah), Tel. +212619725374; email: Badreddinehatimi@gmail.com (B. Hatimi)
[b]_Univ Hassan1, Laboratoire de Chimie et Modélisation Mathématique, Faculté Polydisciplinaire, 25000 Khouribga, Morocco,_
Tel. +212668858296, email: elmhammedi@yahoo.fr

ABSTRACT

In this study, a batch system was applied to investigate the adsorption behavior of disperse dyes (Disperse Blue 79 [DB 79] and Disperse Blue 165 [DB 165]) and an anionic dye (Reactive Yellow 145 [RY 145]) on natural phosphate doped by titanium dioxide (NP-TiO$_2$). The NP-TiO$_2$ was characterized by X-ray diffraction, Fourier transform-infrared and Brunauer–Emmett–Teller surface area techniques. The established optimum contact time for DB 79, DB 165 and RY 145 was 60, 90 and 75 min, respectively, at a dye concentration of 50 mg/L, DB 79, DB 165 and RY 145 dye removal rates reached 97%, 99% and 78%, respectively. Kinetic parameters were estimated using the pseudo-first-order and pseudo-second-order kinetic models, the adsorption rate was fitted by pseudo-second-order model for DB 79 and RY 145. However, the DB 165 was described by pseudo-first-order model. Further investigations demonstrated that the adsorption isotherm fitted well with the Langmuir model for DB 79 and DB 165, but the RY 145 dye was described by the Freundlich model. The thermodynamic parameters were also studied.

Keywords: Disperse Blue 79 (DB 79); Disperse Blue 165 (DB 165); Reactive Yellow 145 (RY 145); Natural phosphate; TiO$_2$; Isotherm model

1. Introduction

Dye wastewater is potentially toxic, carcinogenic and non-biodegradable, which causes enormous environmental concerns [1]. Azo dyes are one of the most widely used chromospheres in the dye chemistry. These dyes can be divided into monoazo, diazo, triazo classes according to the presence of one or more azo bonds (–N=N–) [2]. Azo dyes are very stable and difficult to remove from wastewater because they have complex aromatic structures [3,4]. However, their removal is difficult by conventional wastewater treatment

systems [5]. For this reason, several treatment methods have been developed for this purpose [6], such as coagulation [7,8], chemical oxidation [9–11], photocatalysis [12], electrochemical methods [13] and adsorption [14]. The removal of dyes from wastewater by adsorption has become the best alternative compared with other expensive treatment methods. In recent years, many researchers have developed excellent low cost and environmentally-friendly adsorbents [1,5,15]. Natural phosphate is an abundant resource in Morocco [16], it can be used not only as fertilizers, but also it has been successfully utilized as an adsorbent either

alone or modified to remove dyes from wastewater [17–19]. In this study, Moroccan natural phosphate doped by titanium dioxide was used as an adsorbent to remove disperse and anionic dyes from aqueous solutions.

2. Materials and methods

2.1. Materials

Disperse blue 79, Disperse blue 165 and Reactive yellow 145 were purchased from Sigma-Aldrich (Morocco). The chemical structures of these dyes are shown in Fig. 1. NP was collected from the local phosphate industry located in Khouribga, Morocco, TiO_2 (Degussa P25) was obtained from Ahlstrom Company (France). All other chemicals were used without purification.

2.2. Preparation of NP-TiO$_2$

NP-TiO_2 was synthesized by mixing 0.02 g of TiO_2 (Degussa P25) with 1 g of natural phosphate. The mixture was ground in a mortar and was calcined at different temperatures (200°C, 400°C, 500°C, 600°C, 700°C and 800°C) for 14 h in the oven [20].

2.3. Characterization methods

Wide-angle X-ray diffraction (XRD) patterns were recorded by XPERT-PRO with a K_{Cu} = 1.5406 nm target at a scan rate of 0.02° (2θ) from 15° to 80°. Fourier transform-infrared (FTIR) spectra of samples were recorded with KBr pellet in the range of 4,000–600 cm^{-1} on FTIR, Vertex 70 de BRUKER spectrometer (Rabat, Morocco) at room temperature. The Brunauer–Emmett–Teller (BET) surface area was determined using Autosorb IQ of Quantachrome Instruments (Rabat, Morocco).

2.4. Adsorption experiments

To study the effect of environmental parameters such as adsorbent dose, contact time, initial dye concentration, solution pH and solution temperature for the removal of DB 79, DB 165 and RY 145 using NP-TiO_2, batch experiments were carried out using 100 mL of different initial dyes concentrations (20–100 mg/L) with addition of a specific dose of NP-TiO_2 (0–10 g/L). The pH was adjusted in the range of 4.0–10.0 by concentrated HCl and NaOH. The effect of temperature was studied at temperature ranged between 20°C and 60°C. The NP-TiO_2-adsorbate was then separated by centrifugation. The supernatant solutions were measured with UV–Vis spectrophotometer (Jasco V-630, El Jadida, Morocco) at a maximum wavelength of 537, 540 and 419 nm of DB 79, DB 165 and RY 145, respectively. Each experiment was replicated three times and error bars were presented in all graphs. The removal percentage of dyes (%), capacity of adsorption at equilibrium q_e (mg/g) and at time q_t (mg/g) were computed as follows:

$$\%R = \frac{C_0 - C_e}{C_0} \times 100 \tag{1}$$

$$q_e = \frac{C_0 - C_e}{W} \times V \tag{2}$$

$$q_t = \frac{C_0 - C_t}{W} \times V \tag{3}$$

where C_t is the dye concentration at time t, C_0 (mg/L) is the initial dye concentration, C_e (mg/L) is the dye concentration at equilibrium, V (L) is the volume of dye and W (g) is the amount of the adsorbent in the solution.

3. Results and discussion

3.1. Characterization of NP-TiO$_2$

3.1.1. Chemical composition

The chemical composition of natural phosphate is reported in Table 1. It mostly contains CaO, and P_2O_5 with traces of sodium, potassium, magnesium while Fe_2O_3 and Al_2O_3 are present in low percentages. The ratio of CaO/P_2O_5
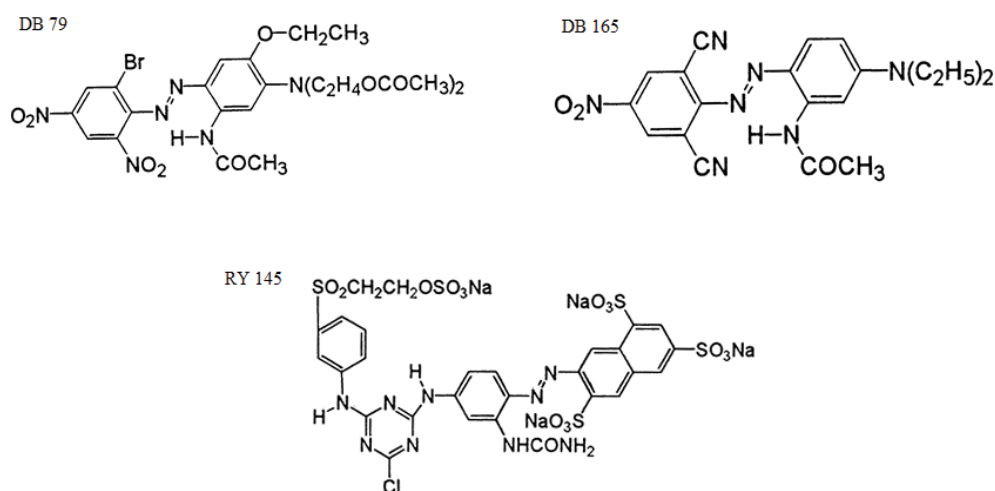

Fig. 1. Chemical structure of investigated dyes.

Table 1
Chemical composition of Moroccan natural phosphate (%)

CaO	54.12
SO_3	2.24
P_2O_5	32.24
CO_2	2.21
Al_2O_3	0.68
Fe_2O_3	0.46
K_2O	0.36
F^-	3.37
MgO	0.92
Na_2O	1.13
SiO_2	2.42

1.67 confirms that the NP used in this study has a carbonated fluorapatite structure.

3.1.2. XRD analysis

The XRD patterns of TiO_2, NP and NP-TiO_2 calcined at different temperatures are presented in Fig. 2a. The analysis of the natural phosphate X-ray diffractogram shows a well crystallized sample which consists mainly of fluorapatite. Two main peaks of TiO_2 were observed at 2θ: 24.3° and 28.4°. The anatase phase was located at 2θ: 24.3° and the rutile phase was seen at 2θ: 28.4°, these two phases are associated with (101) and (110) planes for anatase and rutile, respectively [21].

At temperatures ranging from 200°C to 500°C, the two peaks of anatase and rutile phases remain constant. At 600°C, the rutile peak intensity increased compared with that of the anatase peak intensity that decreased. However, the anatase

phase peaks disappeared at temperatures above 600°C while the rutile phase peak intensities increased [22].

3.1.3. FTIR analysis

The IR absorption spectrum (Fig. 2b) shows the characteristic bands of NP and NP-TiO_2. The spectrum indicated that the NP used in this study had a fluorapatite structure. The bands located between 1,430 and 1,461 cm^{-1} were attributed to carbonated fluorapatite [19]. Moreover, the IR spectrum shows independently the bands of phosphates located between 700 and 1,100 cm^{-1}. However, the bands positioned at 3,500 cm^{-1} in the NP were assigned to hydroxyl stretching mode of vibration [20]. The anatase and rutile characteristic vibration peaks were observed at 1,080 after phosphate modification [23].

3.1.4. BET surface area

The BET surface areas of NP and TiO_2 are 10 is 50 m^2/g, respectively. However, after the surface modification of NP with TiO_2, the specific surface area of NP-TiO_2 calcined from 200°C to 800°C decreased from 28.249 to 7.580 m^2/g; due to the damage of structure of TiO_2 at higher temperatures [20].

3.2. Comparison of the adsorption of dyes by NP, TiO_2 and NP–TiO_2

The adsorption of DB 79, DB 165 and RY 145 onto NP, TiO_2 and NP-TiO_2 at room temperature and different calcined temperatures was performed. The results are shown in Fig. 3. It can be observed that NP-TiO_2 calcined at 600°C exhibited completely different behavior compared with other adsorbents. DB 79 and DB 165 were adsorbed almost completely using NP-TiO_2 calcined at 600°C, however, the adsorption of RY 145 only reached 78%; this is probably
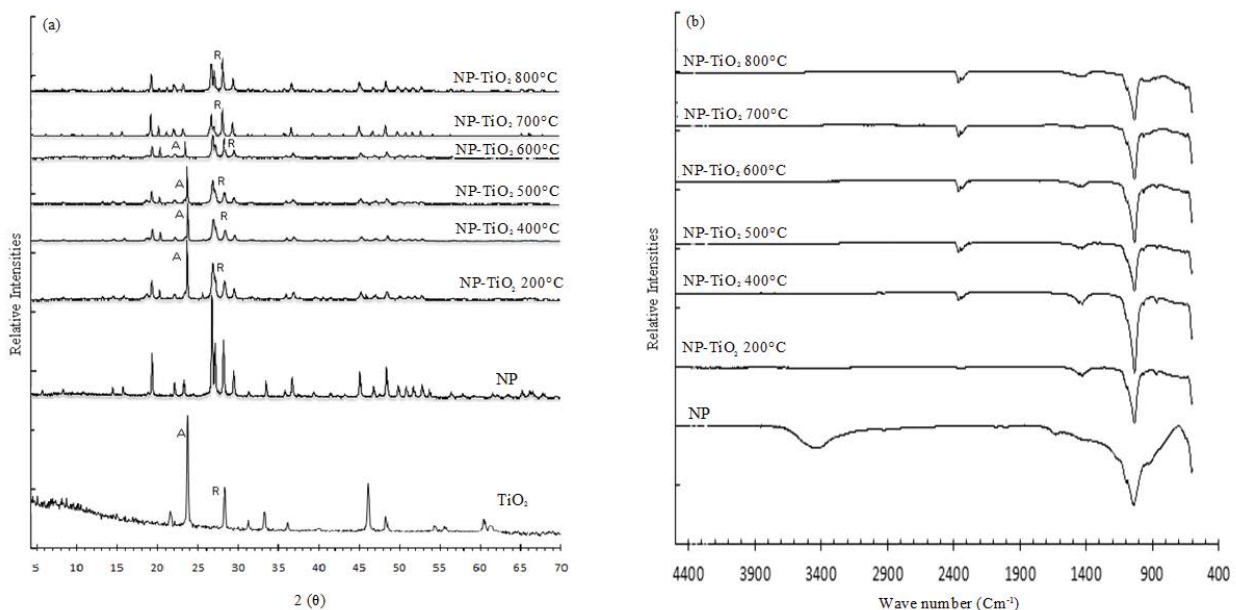

Fig. 2. (a) XRD patterns NP and NP-TiO_2 calcined from 200°C to 800°C (A: anatase phase, R: rutile phase) and (b) FTIR spectra of NP and NP-TiO_2 calcined from 200°C to 800°C.
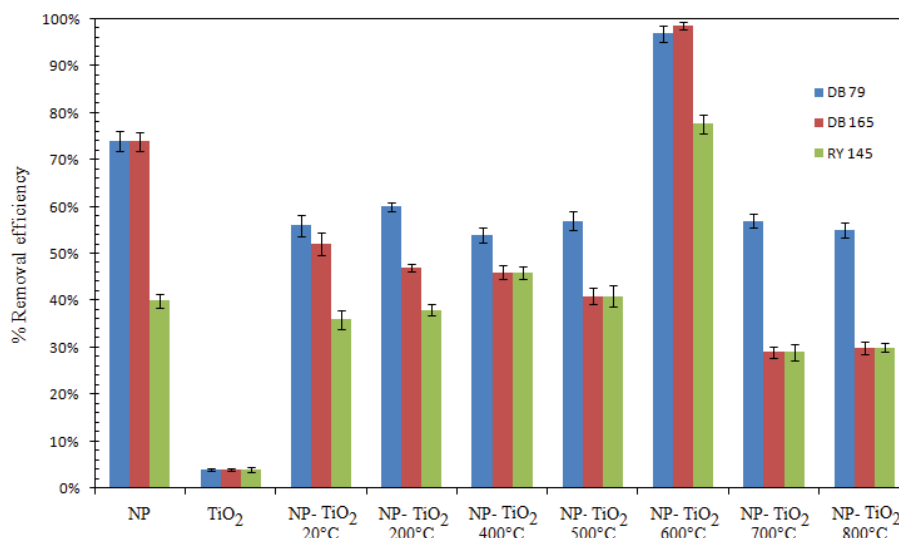
Fig. 3. Adsorption of DB 79, DB 165 and RY 145 by NP, TiO$_2$ and NP-TiO$_2$ at room and different temperatures of calcination (DB79, DB 165 and RY 145 concentration: 50 mg/L; adsorbent dosage: 5 g/L; pH = 6 and time: 135 min).

due to the complex molecular structure of the RY 145 dye compared with that of the DB 79 and DB 165 dye; the molecular weight of DB 79 and DB 165 is 639.416 and 405.41 g/mol, respectively, whereas the molecular weight of RY 145 is 1,026.25 g/mol, for this reason the RY 145 molecules find much difficulty adhering on NP-TiO$_2$ surface compared with DB 79 and DB 165 molecules [24].

The NP-TiO$_2$ calcined at 600°C manifested higher removal percentage (%DB 79 = 97%, %DB 165 = 99% and %RY 145 = 78%) compared with NP (%DB 79 = 70%, %DB 165 = 69% and %RY 145 = 44%), NP-TiO$_2$ non-calcined and calcined at different temperatures; this can be explained by the fact that the NP-TiO$_2$ calcined at 600°C had two phases (anatase and rutile) and considered as last step to convert the anatase to rutile phase [25]. Therefore, the 600°C was chosen as the optimum calcination temperature for the NP-TiO$_2$ adsorbent in this study.

3.3. Effect of contact time

Fig. 4 shows the effect of contact time on the adsorption of DB 79, DB 165 and RY 145 dyes onto NP-TiO$_2$, using a constant adsorbent dose of 5 g/L and initial dyes concentration of 50 mg/L. To ensure maximum removal percentage, 135 min was applied as time of contact for the adsorption experiments. The adsorption rate was rapid during the first 30 min and then gradually decreased reaching a plateau after approximately 60, 90 and 75 min of contact for DB 79, DB 165 and RY 145, respectively. The first rapid adsorption step of the three dyes was due to the large number of vacant surface sites of the adsorbent, and the slower adsorption rate after 30 min was due to sluggish diffusion of dyes into the interior of NP-TiO$_2$.

3.4. Effect of concentration

The effect of the initial DB 79, DB 165 and RY 145 dyes concentration depends on the immediate relation between

dyes and the available binding sites on NP-TiO$_2$ [26]. The effect of the initial dyes concentration on the removal percentage is shown in Fig. 5. The removal uptake of the three dyes decreased with the increase in the initial dyes concentration from 20 to 100 mg/L; at concentrations ranging from 20 to 50 mg/L, the removal percentage was optimal for the three dyes due to vacant sites of the NP-TiO$_2$. Above 50 mg/L, the active sites required for the adsorption of the three dyes will eventually decrease [27,28].

3.5. Effect of adsorbent dose

Fig. 6 shows that initially the removal efficiency of dyes increased rapidly with the increase in adsorbent dose of NP-TiO$_2$, after reaching the optimal dose (5 g/L), the removal
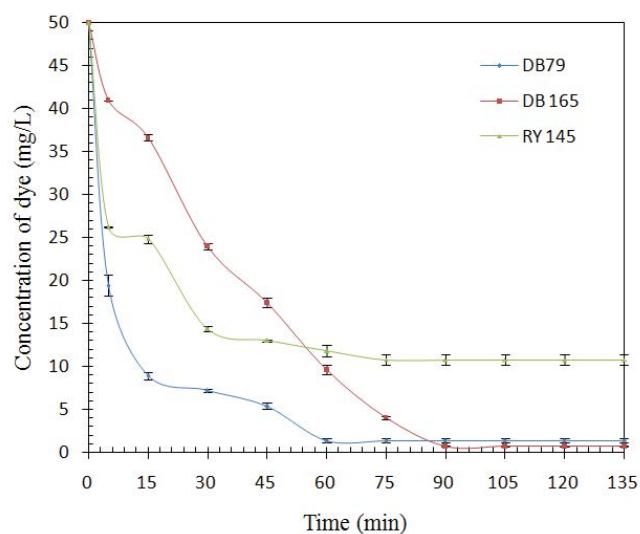

Fig. 4. Effect of contact time of DB 79, DB 165 and RY 145 by NP-TiO$_2$ (dye concentration: 50 mg/L; adsorbent dosage: 5 g/L; pH = 6; T = 20°C).
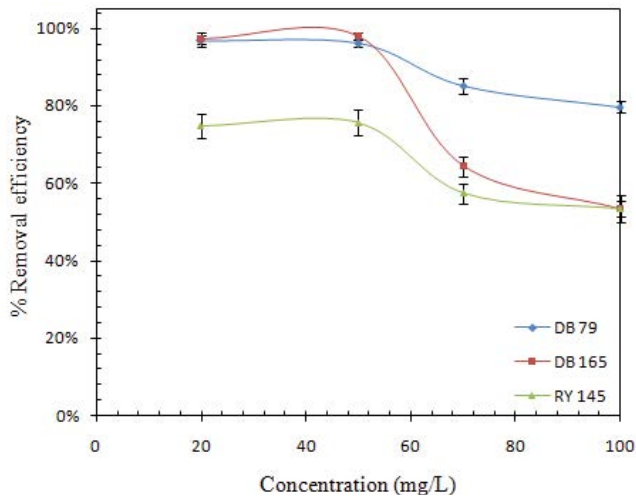
Fig. 5. Effect of initial concentration of DB 79, DB 165 and RY 145 by NP-TiO$_2$ (adsorbent dosage: 5 g/L; pH = 6; T = 20°C).

Fig. 7. Effect of pH of DB 79, DB 165 and RY 145 onto NP-TiO$_2$ (dye concentration 50 mg/L; adsorbent dosage: 5 g/L; T = 20°C).

DB 165. However, the adsorption was found to decrease with increasing pH solution from 6 to 10 for RY 145; it could be explained by the repulsion charges between the negatively charged NP-TiO$_2$ and the negative charge of dye molecules [30].

3.7. Effect of temperature

The effect of solution temperature on the adsorption of DB 79, DB 165 and RY 145 onto NP-TiO$_2$ was studied by measuring the adsorption uptake at various temperatures varying between 20°C and 60°C.

The results are presented in Fig. 8, the removal efficiency of DB 79, DB 165 and RY 145 increased as the temperature
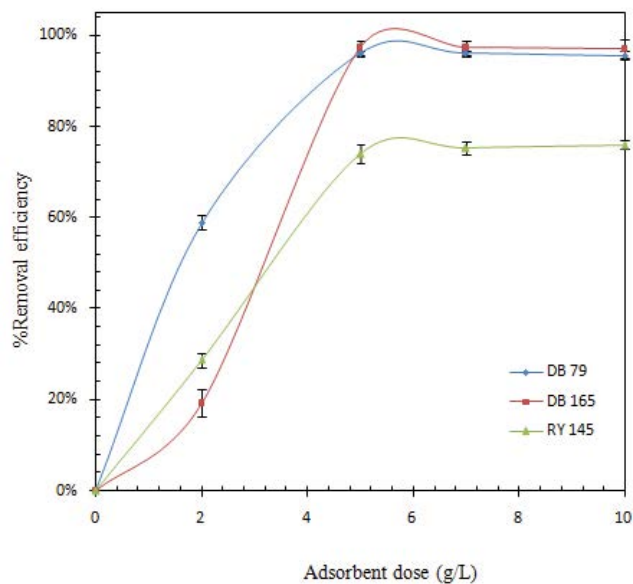

Fig. 6. Effect of adsorbent dose of DB 79, DB 165 and RY 145 using NP-TiO$_2$ as adsorbent (dye concentration: 50 mg/L; pH = 6; T = 20°C).

efficiency became constant. The DB 79 removal efficiency increased from 60% to 97%, from 16% to 99% for DB 165 and from 27% to 78% for RY 145 by increasing the adsorbent dose from 0 to 10 g/L. The increase of the adsorbent dose multiplied the number of vacant adsorption sites, thus leading to an increase in the removal uptake [29]. Consequently, 5 g/L was chosen as optimal dose for all further studies.

3.6. Effect of solution pH

The variation of removal percentages at different pH values for DB 79, DB 165 and RY 145 removal is shown in Fig. 7. There was no significant decrease in the dyes uptake when varying the solution pH from 4 to 10 for DB 79 and
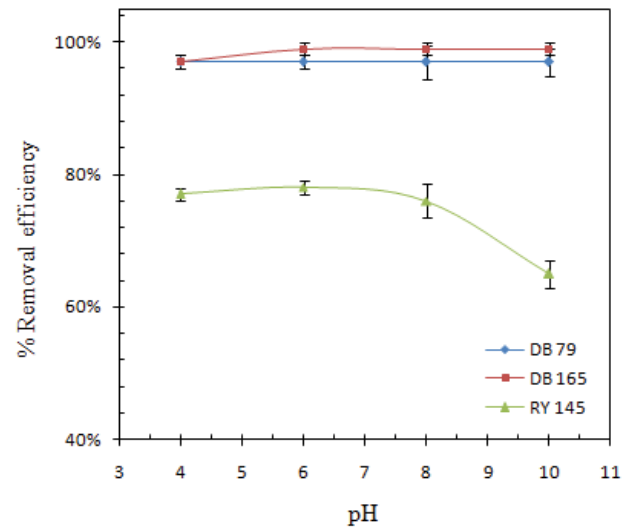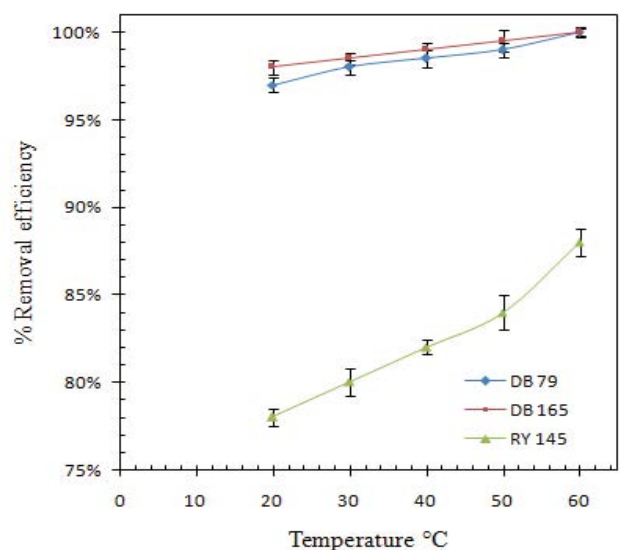

Fig. 8. Effect of temperature of DB 79, DB 165 and RY 145 onto NP-TiO$_2$ (dye concentration 50 mg/L; adsorbent dosage: 5 g/L; pH = 6).

increased from 20°C to 60°C. These results revealed that DB 79, DB 165 and RY 145 removal was endothermic [31].

3.8. Adsorption kinetics

Adsorption kinetics was investigated to understand the interactions of adsorbate–adsorbent system. The linearized forms of pseudo-first-order and pseudo-second-order kinetic equations are given as Eqs. (4) and (5), respectively [32–34]:

$$\log\left(q_e - q_t\right) = \log q_e - \frac{K_1}{2.303}t \tag{4}$$

$$\frac{t}{q_t} = \frac{1}{K_2 q_e^2} + \frac{t}{q_e} \tag{5}$$

where K_1 (min⁻¹) and K_2 (g/mg min) are the rate constants of the adsorption process for pseudo-first-order and pseudo-second-order respectively, while q_e (mg/g) and q_t (mg/g) are the adsorption capacities at equilibrium, and at time t (min).

Figs. 9a and b show the linear plot of $\log\left(q_e - q_t\right)$ vs. t and t/q_t vs. t. Table 2 shows that the experimental data fitted better with the pseudo-second-order kinetic model compared with the pseudo-first-order kinetic model for DB 79 and RY 145 with $R^2 > 0.99$, the table also shows good agreement between the experimental and the calculated adsorption capacities for DB 79 and RY 145 dyes. However, the experimental data

fitted best with pseudo-first-order for DB 165 with $R^2 = 0.95$, furthermore, the experimental adsorption capacity was close to that calculated by pseudo-first-order.

3.9. Adsorption isotherms

The adsorption isotherm describes the interaction between the adsorbent and the adsorbate, and gives a comprehensive understanding of the nature of interaction. Several isotherm equations were developed and used for such analysis; two important isotherms were investigated in this study, Langmuir and Freundlich isotherm models.

Langmuir isotherm can be represented as follows [35–37]:

$$\frac{C_e}{q_e} = \frac{1}{K_L q_m} + \frac{1}{q_m}C_e \tag{6}$$

where q_e and C_e are the adsorption capacity (mg/g) and the dye concentration (mg/L) at equilibrium, respectively, q_m represents the maximum adsorption capacity of the adsorbent (mg/g) and K_L the Langmuir adsorption constant (L/mg). The values of q_m and K_L are calculated from the slope and intercept of the linear plot of $1/q_e$ against $1/C_e$.

The Freundlich isotherm is a special model for heterogeneous surface energy of adsorption [37]. It can be described as:
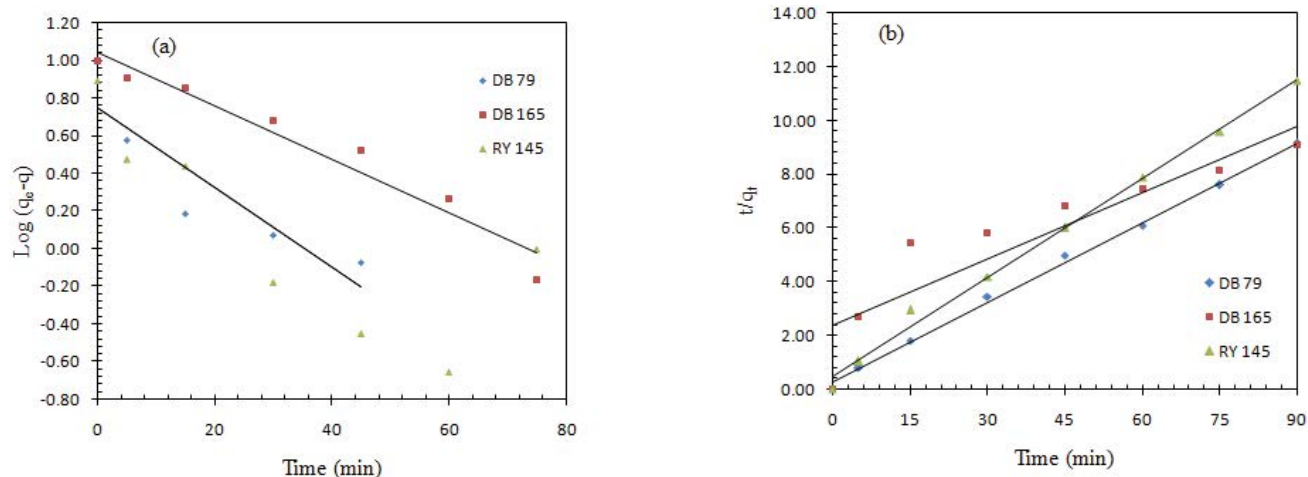
$$q_e = K_F C_e^{1/n} \tag{7}$$

Fig. 9. (a) Pseudo-first-order kinetics of dyes adsorption and (b) Pseudo-second-order kinetics of dyes adsorption onto NP-TiO$_2$ at 20°C, adsorbent dose 5 g/L and 50 mg/L of initial dye concentration.

Table 2
Pseudo-first-order and pseudo-second-order kinetic parameters for the adsorption of DB 79, DB 165 and RY 145 onto NP-TiO$_2$ (temperature: 20°C; pH: 6, 5 g/L and 50 mg/L of initial dye concentration)

| Adsorbate | Concentration (mg/L) | Pseudo-first-order | | | | Pseudo-second-order | | |
		$q_{e,\exp}$ (mg/g)	$q_{e,\text{calc}}$ (mg/g)	K_1 (min⁻¹)	R^2	$q_{e,\text{calc}}$ (mg/g)	K_2 (g/mg min)	R^2
DB 79	50	9.867	5.598	0.048	0.807	10.204	0.035	0.997
DB 165	50	9.893	11.066	0.032	0.951	12.195	0.003	0.824
RY 145	50	7.844	3.741	0.035	0.601	8.197	0.031	0.994

where K_F is the adsorption capacity at unit concentration and $1/n$ is the adsorption intensity. The $1/n$ value ranges between 0 and 1 and it is a measure of surface heterogeneity. Also, it indicates the type of isotherm to be irreversible ($1/n = 0$), favorable ($0 < 1/n < 1$) and unfavorable ($1/n > 1$). K_F and n can be obtained from the intercept and the slope of the linear plot of $\ln q_e$ vs. $\ln C_e$.

The best-fit model was selected based on the linear regression correlation coefficient values (R^2); which must be higher than 0.90 [38].

Fig. 10 shows the equilibrium isotherms for DB 79, DB 165 and RY 145 adsorption by NP-TiO$_2$. The adsorption of DB 79 and DB 165 using NP-TiO$_2$ was well fitted by the Langmuir isotherm model (R^2 were 0.97 and 0.975 for DB 79 and DB 165, respectively), indicating a monolayer adsorption of dyes on the surface of NP-TiO$_2$. The correlation coefficients and the adsorption capacities of both dyes are shown in Table 3.

The Freundlich isotherm model gave the highest R^2 values (greater than 0.97 for RY 145), this shows that the adsorption of RY 145 onto NP-TiO$_2$ was best described by this model. The values of $1/n$ presented in Table 3 shows that the adsorption was favorable for the three dyes.

3.10. Adsorption thermodynamics

The thermodynamic parameters of adsorption process such as standard Gibbs free energy change ($\Delta G°$), standard enthalpy change ($\Delta H°$) and standard entropy change ($\Delta S°$), were calculated using Eqs. (8) and (9) [39,40]:

$$\Delta G° = -RT \ln K_a \tag{8}$$

and

$$\ln K_a = -\frac{\Delta H°}{RT} + \frac{\Delta S°}{R} \tag{9}$$

where R (8.314 J/mol K) is the gas constant, T (K) is the absolute temperature, and K_a has no unit, is the standard thermodynamic equilibrium constant determined from the Langmuir isotherm model [41]:

$$q_e = q_{max} \frac{C_e K_L}{C_e K_L + 1} \tag{10}$$

where C_e is the concentration at equilibrium (mmol/L), q_{max} is the capacity of adsorption obtained from Langmuir model and K_L is the Langmuir adsorption constant (L/mmol). The slope and intercept of the linear plot of $\ln (K_a)$ vs. $1/T$ (Fig. 11) provided the values of $\Delta H°$ and $\Delta S°$.

The obtained $\Delta G°$, $\Delta H°$ and $\Delta S°$ for the adsorption of DB 79, DB 165 and RY 145 onto NP-TiO$_2$ are listed in Table 4. The values of $\Delta H°$ are positive for all dyes, which indicate that the adsorption processes are endothermic in nature [42].
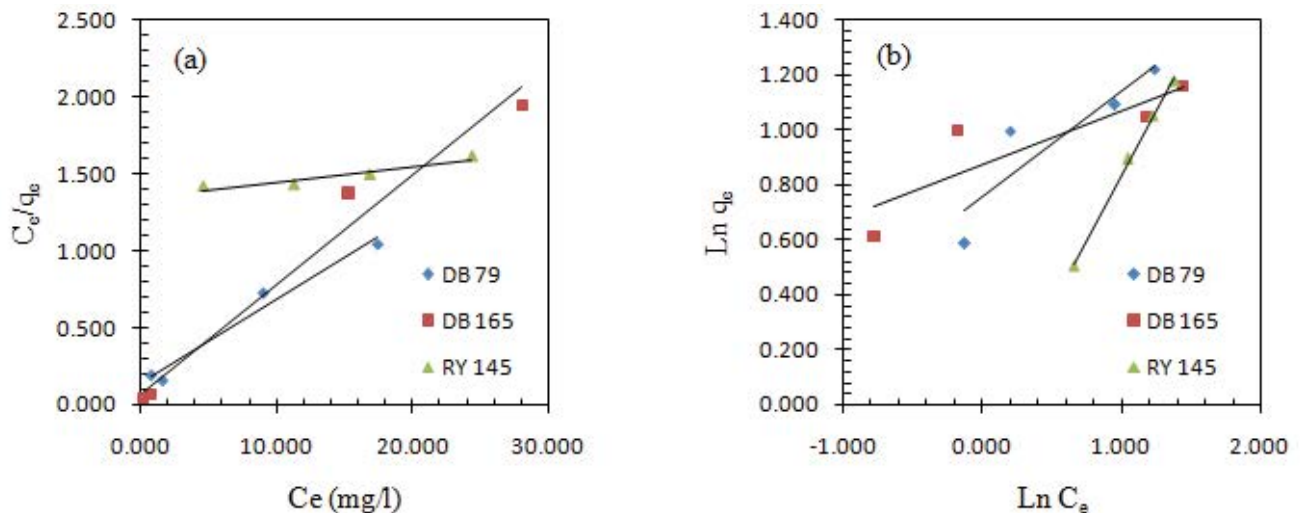

Fig. 10. (a) Langmuir isotherm of dyes adsorption and (b) Freundlich isotherm of dyes adsorption onto NP-TiO$_2$ at 20°C, adsorbent dose 5 g/L and 50 mg/L of initial dye concentration.

Table 3
Langmuir and Freundlich isotherms parameters for the adsorption of DB 79, DB 165 and RY 145 onto NP-TiO$_2$ (at 20°C, dye: 50 mg/L; pH: 6; adsorbent dose 5 g/L)

	Freundlich				Langmuir		
	k	N	$1/n$	R^2	K_L (L/mg)	q (mg/g)	R^2
DB 79	5.649	2.571	0.389	0.814	0.386	18.519	0.970
DB 165	7.413	5.128	0.195	0.764	0.933	14.286	0.975
RY 145	0.794	1.053	0.95	0.977	0.037	33.333	0.900

Table 4
Equilibrium constant and Gibbs free energy of adsorption of DB 79, DB 165 and RY 145 on NP-TiO$_2$

Adsorbate	$\Delta G°$ kJ/mol					$\Delta H°$ kJ/mol	$\Delta S°$ kJ/mol K
	293	303	313	323	333		
DB 79	−20.33	−22.89	−25.21	−27.24	−30.45	51.51	0.25
DB 165	−20.33	−22.04	−24.77	−26.47	−30.71	53.18	0.25
RY 145	−17.43	−18.70	−19.56	−20.65	−21.58	12.56	0.10

Table 5
Comparison of the adsorption capacities of DB 79, DB 165 and RY 145 dyes onto different adsorbents in literature

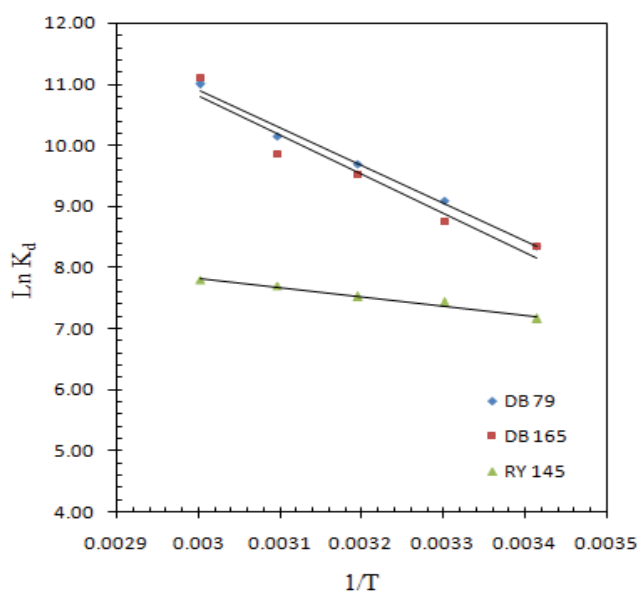| Adsorbent	Adsorbate	Capacity of adsorption mg/g	% Removal	Reference
Fly ash	DB 79	3.26	–	[43]
Phosphogypsum	DB 165	6.79	–	[44]
Chitosan-coated magnetite nanoparticles	RY 145	47.62	–	[45]
Activated carbon	RY 145	–	90.7	[46]
Treated watermelon seeds	RY 145	115		[47]
NP-TiO$_2$	DB 165	14.286	99	Current study
NP-TiO$_2$	RY 145	33.333	97	Current study
NP-TiO$_2$	DB 79	18.519	78	Current study

Fig. 11. Van't Hoff plot for the adsorption of DB 79, DB 165 and RY 145 onto NP-TiO$_2$.

In addition, adsorption of DB 79 and DB 165 onto NP-TiO$_2$ was spontaneous and favorable at all the experimental temperatures as a result of negative values of $\Delta G°$. It was also noted that the values of $\Delta G°$ decreased by increasing temperature, which indicates that the adsorption was more favorable at higher temperatures. The positive values of $\Delta S°$ indicate an increase in randomness at the solid–solution interface.

3.11. Comparison study of the adsorption of DB79, DB 165 and RY 145 using different adsorbents

The adsorption capacities of DB 79, DB 165 and RY 145 removal using different adsorbents is shown in Table 5; the adsorption performance of the NP-TiO$_2$ prepared in this study was higher than other adsorbents used in different studies for DB 79 and DB 165.

4. Conclusion

NP-TiO$_2$ was successfully used as adsorbent for the adsorption of DB 79, DB 165 and RY 145. Adsorption isotherms and kinetics explained well the adsorption mechanisms for the three dyes. The composite was characterized using XRD, FTIR spectroscopy and BET. Equilibrium isotherm data fitted well with Langmuir isotherm data for DB 79 and DB 165, however, the adsorption of RY 145 onto NP-TiO$_2$ fitted best with Freundlich isotherm model. The DB 79 and RY 145 adsorption was well described by the pseudo-second-order kinetic model while the adsorption of DB 165 fitted best with pseudo-first-order model. The optimum conditions were noted at 5.0 g/L of adsorbent dose, 50 mg/L of initial dye concentration and 60°C of temperature for the three studied dyes. The results suggested that NP-TiO$_2$ is a promising adsorbent for the successful removal of DB 79, DB 165 and RY 145 from aqueous solution.

References

[1] V.K. Gupta, Suhas, Application of low-cost adsorbents for dye removal: a review, J. Environ. Manage., 90 (2009) 2313–2342.
[2] S. Garcia-Segura, E. Brillas, Combustion of textile monoazo, diazo and triazo dyes by solar photoelectro-Fenton: decolorization,

kinetics and degradation routes, Appl. Catal., B, 181 (2016) 681–691.

[3] G. Crini, Non-conventional low-cost adsorbents for dye removal: a review, Bioresour. Technol., 97 (2006) 1061–1085.

[4] E.R. García, R.L. Medina, M.M. Lozano, I. Hernández Pérez, M.J. Valero, A.M.M. Franco, Adsorption of azo-dye Orange II from aqueous solutions using a metal-organic framework material: iron- benzenetricarboxylate, Mater, 7 (2014) 8037–8057.

[5] P. Leechart, W. Nakbanpote, P. Thiravetyan, Application of waste wood-shaving bottom ash for adsorption of azo reactive dye, J. Environ. Manage., 90 (2009) 912–920.

[6] V.K. Gupta, I. Ali, T.A. Saleh, A. Nayak, S. Agarwal, Chemical treatment technologies for waste-water recycling: an overview, RSC Adv., 2 (2012) 6380–6388.

[7] C.C. Mólgora, A.M. Domínguez, E.M. Avila, P. Drogui, G. Buelna, Removal of arsenic from drinking water: a comparative study between electrocoagulation-microfiltration and chemical coagulation-microfiltration processes, Sep. Purif. Technol., 118 (2013) 645–651.

[8] M. Tiaiba, B. Merzouk, A. Amour, M. Mazour, J.-P. Leclerc, F. Lapicque, Influence of electrodes connection mode and type of current in electrocoagulation process on the removal of a textile dye, Desal. Wat. Treat., 73 (2017) 330–338.

[9] I.A. Salem, M.S. El-Maazawi, Kinetics and mechanism of color removal of methylene blue with hydrogen peroxide catalyzed by some supported alumina surfaces, Chemosphere, 41 (2000) 1173–1180.

[10] A.A. Zorpas, Chemical oxidation and Membrane Bioreactor for the treatment of Household heating wastewater, Desal. Wat. Treat., 51 (2013) 6952–6960.

[11] M. Muthukumar, D. Sargunamani, M. Senthilkumar, N. Selva-kumar, Studies on decolouration, toxicity and the possibility for recycling of acid dye effluents using ozone treatment, Dyes Pigm., 64 (2005) 39–44.

[12] H. Zhang, G. Wang, D. Chen, X. Lv, J. Li, Tuning photo-electrochemical performances of Ag–TiO$_2$ nanocomposites via reduction/oxidation of Ag, Chem. Mater., 20 (2008) 6543–6549.

[13] N.N. Rao, K.M. Somasekhar, S.N. Kaul, L. Szpyrkowicz, Electrochemical oxidation of tannery wastewater, J. Chem. Technol. Biotechnol., 76 (2001) 1124–1131.

[14] S. Kaur, S. Rani, R.K. Mahajan, Adsorption of dye crystal violet onto surface-modified Eichhornia crassipes, Desal. Wat. Treat., 53 (2015) 1957–1969.

[15] G. Enaime, K. Ennaciri, A. Ounas, A. Baçaoui, M. Seffen, T. Selmi, A. Yaacoubi, Preparation and characterization of activated carbons from olive wastes by physical and chemical activation: application to Indigo carmine adsorption, J. Mater. Environ. Sci., 8 (2017) 4125–4137.

[16] S.Y. Rahni, K. Sharafie, H. Biglari, Mucilage of plantago ovata as natural coagulation–flocculation aid in an electrocoagulation process for phosphate removal from aqueous environments, Desal. Wat. Treat., 99 (2017) 282–288.

[17] S. Sebti, A. Solhy, R. Tahir, S. Boulaajaj, J.A. Mayoral, J.M. Fraile, A. Kossirc, H. Oumimoun, Calcined sodium nitrate/natural phosphate: an extremely active catalyst for the easy synthesis of chalcones in heterogeneous media, Tetrahedron Lett., 42 (2001) 7953–7955.

[18] A. Lamhamdi, K. Azzaoui, E. Mejdoubi, B. Hammouti, M. Berrabah, M. Zegmout, B. Razzouki, Contribution of adsorption of metals using calcium phosphates in the presence of support polyethylene glycol, J. Mater. Environ. Sci., 5 (2014) 2584–2589.

[19] N. Barka, A. Assabbane, A. Nounah, L. Laanab, Y.A. Ichou, Removal of textile dyes from aqueous solutions by natural phosphate as a new adsorbent, Desalination, 235 (2009) 264–275.

[20] N. Naciri, A. Farahi, S. Rafqah, H. Nasrellah, M.A. El Mhammedi, I.T. Lançar, M. Bakasse, Effective photocatalytic decolorization of indigo carmine dye in Moroccan natural phosphate–TiO$_2$ aqueous suspensions, Opt. Mater., 52 (2016) 38–43.

[21] C. Bernardini, G. Cappelletti, M.V. Dozzi, E. Selli, Photocatalytic degradation of organic molecules in water: photoactivity and reaction paths in relation to TiO$_2$ particles features, J. Photochem. Photobiol., A, 211 (2010) 185–192.

[22] A.A. Umar, M.Y.A. Rahman, S.K.M. Saad, M.M. Salleh, Effect of NH$_3$ concentration on the performance of nitrogen doped TiO$_2$ photoelectrochemical cell, Int. J. Electrochem. Sci., 7 (2012) 7855–7865.

[23] D. Zhao, C. Chen, Y. Wang, H. Ji, W. Ma, L. Zang, J. Zhao, Surface modification of TiO$_2$ by phosphate: effect on photocatalytic activity and mechanism implication, J. Phys. Chem. C, 112 (2008) 5993–6001.

[24] R. Malarvizhi, Y.-S. Ho, The influence of pH and the structure of the dye molecules on adsorption isotherm modeling using activated carbon, Desalination, 264 (2010) 97–101.

[25] R. Fagan, D.E.M. Cormack, S.J. Hinder, S.C. Pillai, Improved high temperature stability of anatase TiO$_2$ photocatalysts by N, F, P co-doping, Mater. Des., 96 (2016) 44–53.

[26] S.A. Umoren, U.J. Etim, A.U. Israel, Adsorption of methylene blue from industrial effluent using poly (vinyl alcohol), J. Mater. Environ. Sci., 4 (2013) 75–86.

[27] N. Barka, S. Qouzal, A. Assabbane, A. Nounhan, Y.A. Ichou, Removal of reactive yellow 84 from aqueous solutions by adsorption onto hydroxyapatite, J. Saudi Chem. Soc., 15 (2011) 263–267.

[28] M. Kumar, R. Tamilarasan, V. Sivakumar, Adsorption of Victoria blue by carbon/Ba/alginate beads: kinetics, thermodynamics and isotherm studies, Carbohydr. Polym., 98 (2013) 505–513.

[29] Y. Ren, H.A. Abbood, F. He, H. Peng, K. Huang, Magnetic EDTA-modified chitosan/SiO$_2$/Fe$_3$O$_4$ adsorbent: preparation, characterization, and application in heavy metal adsorption, Chem. Eng. J., 226 (2013) 300–311.

[30] L. Obeid, A. Bee, D. Talbot, S.B. Jaafar, V. Dupuis, S. Abramson, V. Cabuil, M. Welschbillig, Chitosan/maghemite composite: a magsorbent for the adsorption of methyl orange, J. Colloid Interface Sci., 410 (2013) 52–58.

[31] Q.H. Hu, S.Z. Qiao, F. Haghseresht, M.A. Wilson, G.Q. Lu, Adsorption study for removal of Basic Red Dye using bentonite, Ind. Eng. Chem. Res., 45 (2006) 733–738.

[32] J.X. Lin, S.L. Zhan, M.H. Fang, X.Q. Qian, H. Yang, Adsorption of basic dye from aqueous solution onto fly ash, J. Environ. Manage., 87 (2008) 193–200.

[33] M. Monier, D.M. Ayad, Y. Wei, A.A. Sarhan, Adsorption of Cu (II), Co(II), and Ni(II) ions by modified magnetic chitosan chelating resin, J. Hazard. Mater., 177 (2010) 962–970.

[34] H. Zhu, R. Jiang, L. Xiao, L. Liu, C. Cao, G. Zeng, Cd Snano-crystals/TiO$_2$/crosslinked chitosan composite: facile preparation, characterization and adsorption-photocatalytic properties, Appl. Surface Sci., 273 (2013) 661–669.

[35] I. Langmuir, The adsorption of gases on plane surfaces of glass, mica and platinum, J. Am. Chem. Soc., 40 (1918) 1361–1403.

[36] M.N. Ashiq, M. Najam-Ul-Haq, T. Amanat, A. Saba, A.M. Qureshi, M. Nadeem, Removal of methylene blue from aqueous solution using acid/base treated rice husk as an adsorbent, Desal. Wat. Treat., 49 (2012) 376–383.

[37] H. Freundlich, over the adsorption in solution, J. Phys. Chem., 57 (1906) 385–470.

[38] A. Kaushal, S.K. Singh, Critical analysis of adsorption data statistically, Appl. Water Sci., 7 (2017) 3191–3196

[39] I.A.W. Tan, A.L. Ahmad, B.H. Hameed, Adsorption isotherms, kinetics, thermodynamics and desorption studies of 2,4,6-trichlorophenol on oil palm empty fruit bunch-based activated carbon, J. Hazard. Mater., 164 (2009) 473–482.

[40] C. Zhang, S. Yang, H. Chen, H. He, C. Sun, Adsorption behavior and mechanism of reactive brilliant red X-3B in aqueous solution over three kinds of hydrotalcite-like LDHs, Appl. Surf. Sci., 301 (2014) 329–337.

[41] Y. Liu, Is the free energy change of adsorption correctly calculated?, J. Chem. Eng. Data, 54 (2009) 1981–1985.

[42] X. Wei, N. Gao, C. Li, J. Deng, Y. Zhu, Q. Wang, Adsorption of bentazon on two kinds of granular activated carbons: equilibrium, kinetic and thermodynamic studies, Desal. Wat. Treat., 57 (2016) 28762–28775.

[43] H. Hafdi, J. Mouldar, M. Joudi, H. Nasrellah, M.A. El Mhammedi, M. Bakasse, Kinetic, equilibrium and thermodynamic modeling of disperse dye adsorption onto fly ash, Int. J. Adv. Res., 6 (2017) 816–824.

[44] J. Mouldar, M. Joudi, H. Hafdi, H. Nasrellah, L. El Gaini, M. Bakasse, Isotherm, kinetic and thermodynamic studies on the adsorption behavior of disperse blue 165 dye onto chitosan and phosphogypsum, Global J. Eng. Sci. Res. Manage., 4 (2017) 69–78.

[45] N.A. Kalkan, S. Aksoy, E.A. Aksoy, N. Hasirci, Adsorption of reactive yellow 145 onto chitosan coated magnetite nanoparticles, J. Appl. Polym. Sci., 124 (2012) 576–584.

[46] A.H. Sulaymon, W.M. Abood, Removal of reactive yellow dye by adsorption onto activated carbon using simulated wastewater, Desal. Wat. Treat, 52 (2014) 3421–3431.

[47] S. Benkaddour, R. Slimani, H. Hiyane, I. El Ouahabi, I. Hachoumi, S. El Antri, S. Lazar, Removal of reactive yellow 145 by adsorption onto treated watermelon seeds: kinetic and isotherm studies, Sustainable Chem. Pharm., 10 (2018) 16–21.